Ore Geology Reviews 37 (2010) 31–40

Contents lists available at ScienceDirect

Ore Geology Reviews

journal homepage: www.elsevier.com/locate/oregeorev

Origin of the CO_2-only fluid inclusions in the Palaeoproterozoic Carará vein-quartz gold deposit, Ipitinga Auriferous District, SE-Guiana Shield, Brazil: Implications for orogenic gold mineralisation

Evandro L. Klein [a,*], Kazuo Fuzikawa [b]

[a] CPRM/Geological Survey of Brazil, Av Dr. Freitas, 3645, Belém-PA, CEP 66095-110, Brazil
[b] CDTN/CNEN, Rua Mario Werneck s/n, Cidade Universitária, Belo Horizonte-MG, CEP 30270-010, Brazil

ARTICLE INFO

Article history:
Received 12 April 2009
Received in revised form 31 October 2009
Accepted 31 October 2009
Available online 6 November 2009

Keywords:
CO_2-rich fluid inclusions
Gold deposit
Quartz vein
Shear zone
Guiana Shield
Brazil

ABSTRACT

The Carará gold deposit, located in the Ipitinga Auriferous District, south-eastern portion of the Guiana Shield, northern Brazil, is a typical orogenic, greenstone-hosted, auriferous quartz vein. Mineralisation was post-metamorphic and syn-tectonic in relation to the host Palaeoproterozoic (ca. 2.03 Ga) shear zone developed close to the tectonic boundary between a Palaeoproterozoic continental arc and an Archaean block. The deposit style is very simple, consisting of a quartz vein and its hydrothermal envelope, which is composed of muscovite and tourmaline; sulphides are rare. Muscovite and tourmaline, in addition to gold, fill small fractures in the quartz vein. The fluid inclusion assemblage trapped in high- and low-grade portions of the Au–quartz vein is rather enigmatic, consisting of one-phase CO_2 inclusions with no visible water at room or sub-zero temperatures, although small amounts of water have been detected by micro-Raman analysis. In this aspect Carará differs from the other gold showings in the same district, which are characterized by abundant aqueous-carbonic fluid inclusions.

The carbonic fluid is composed predominantly of CO_2 in addition to <2 mol.% N_2 and traces of CH_4 and C_2H_6. The carbonic fluid show very variable densities, which is interpreted to result from post-entrapment re-equilibration. Inclusions in the high-grade quartz are the densest (0.89 to 1.07 g/cm^3) and with less effects of re-equilibration. These inclusions approximate the physico-chemical characteristics of the parental fluid that started to be trapped at least around the amphibolite facies metamorphic conditions and then followed a retrograde path. Most of the inclusions appear to have been trapped and/or re-equilibrated at 350 to 475 °C and 1.8 to 3.6 kbar, which implies a 7 to 12 km depth of vein formation and gold mineralisation. Both phase separation of a carbonic-aqueous fluid (XCO_2>0.8) and the existence of an originally CO_2-dominated fluid could account for the observed fluid inclusion properties and the absence of H_2O-bearing inclusions in the mineralised vein.

The fluid inclusion characteristics, combined with published geological and isotopic information, indicate a deep-seated source for CO_2 that could be mantle, magmatic or metamorphic in origin. We suggest that the likely sources are fluid produced by the 2.07 Ga-old charnockites that occur in the region and/or the coeval high grade metamorphism that is widespread in the Guiana Shield.

1. Introduction

Carbon dioxide-rich fluid inclusions lacking visible H_2O at room temperature are a ubiquitous feature of gold–quartz vein deposits hosted in greenschist to lower amphibolite sequences worldwide. These inclusions occur, in general, as a subordinate population, in close association with cogenetic aqueous-carbonic fluid inclusions. The source and origin of CO_2-rich inclusions and their role in ore-forming processes have been issues of debate. The origin of these CO_2-rich fluid inclusions is usually attributed to: (1) the unmixing of immiscible, low salinity H_2O–CO_2-bearing fluids at or near the solvus followed by post-metamorphic extraction of H_2O and preferential trapping of CO_2 fluids (Crawford and Hollister, 1986; Ho, 1987; Schwartz et al., 1992); (2) post-entrapment changes that include dynamic recrystallisation or strain-induced leakage of H_2O and diffusion of H_2O along dislocation lines (Crawford and Hollister, 1986; Hollister, 1990; Bakker and Jansen, 1991; Johnson and Hollister, 1995); or (3) some combination of these mechanisms (Kolb et al., 2000; Klein et al., 2006). In most cases, however, aqueous and/or cogenetic aqueous-carbonic inclusions are also present.

A few cases have been documented in which CO_2 inclusions are the predominant or even the unique inclusion type. In these cases, again,

* Corresponding author. Tel.: +55 91 3182 1334; fax: +55 91 3276 4020.
E-mail address: eklein@be.cprm.gov.br (E.L. Klein).

0169-1368/$ – see front matter © 2009 Elsevier B.V. All rights reserved.
doi:10.1016/j.oregeorev.2009.10.001

selective entrapment of CO_2 following the unmixing of a H_2O–CO_2 fluid (Garba and Akande, 1992; Xu and Pollard, 1999), and post-entrapment changes (Klemd and Hirdes, 1997; Wille and Klemd, 2004) are the explanations used to describe the observed characteristics of the fluid inclusions. Alternatively, Schmidt-Mumm et al. (1997) and Chi et al. (2009) suggested that the high CO_2 contents could represent an individual category of deep-seated crustal fluids formed at high temperature, e.g., during granulite facies metamorphism.

The source of CO_2 in gold deposits in metamorphic terranes has usually been considered as relics of mantle and/or lower crustal (magmatic and/or metamorphic) fluids (e.g., Phillips and Powell, 1993; Klemd and Hirdes, 1997; Schmidt-Mumm et al., 1997; Lowenstern, 2001) that might have been transported to higher levels in the crust during magma ascent (Xavier and Foster, 1999) and/or channelled along major structures (Chi et al., 2009). Devolatilisation of supracrustal sequences during prograde metamorphism is the more accepted hypothesis for the origin of CO_2 in this type of deposits (Phillips and Powell, 1993; Kerrick and Caldera, 1998). Alternatively, CO_2-dominated fluids may exsolve from felsic magmas formed at depths greater than 5 km in the crust; they are a typical feature of intrusion-related deposits (Baker, 2002). Furthermore, these fluids are also associated with granulite facies metamorphism and with charnockitic magmatism (Santosh et al., 1991; Wilmart et al., 1991).

Carará, in the south-eastern part of the Guiana Shield, northern Brazil, is a typical structurally-controlled gold–quartz vein deposit hosted in a greenschist to lower amphibolite facies metamorphic terrain. The deposit shares a series of geological characteristics with other nearby orogenic gold showings in the Ipitinga Auriferous District (Fig. 1; Klein and Rosa-Costa, 2003; Klein et al., in press). Petrographic examination of quartz vein samples from different portions of the Carará deposit has shown that dark, one-phase CO_2 inclusions with no visible water at room temperature are almost the unique fluid inclusion population occurring in these samples. In this aspect, Carará differs from the other gold occurrences of the Ipitinga District that are characterized by abundant aqueous-carbonic fluid inclusions (Klein et al., in press). The Carará deposit therefore provides a singular opportunity to discuss the origin of the high CO_2 contents in the fluid inclusions and the relationship of this fluid with gold mineralisation. These issues are addressed in the present paper.

2. Geological setting

The Ipitinga Auriferous District is located in the south-eastern portion of the Guiana Shield (Fig. 1), in the border area between the Pará and Amapá states of northern Brazil. This area is part of the large (>1000 km) Palaeoproterozoic Maroni–Itacaiunas orogenic belt (Tassinari and Macambira, 1999). The Ipitinga Auriferous District lies at the boundary between two tectonic terranes — the Carecuru Domain and the Amapá Block (Fig. 1; Rosa-Costa et al., 2009).

According to Rosa-Costa et al. (2009), the Amapá Block consists of an Archaean high-grade association composed of: (1) granulitic gneisses of the Jari–Guaribas Complex (2.80 Ga) (except where stated differently, all reported ages were obtained by the single zircon Pb-evaporation method), represented by orthoderived enderbitic and charnockitic gneisses that enclose minor slivers of mafic and pellitic granulites; (2) mesoperthite- and/or clinopyroxene-bearing granitic gneisses of unknown age that underwent upper-amphibolite to granulite facies metamorphism, included in the Baixo Mapari Complex; (3) granulite facies metasedimentary (aluminous) gneisses and schists of the Iratapuru Complex; (4) amphibolite facies grey gneisses of the Guianense Complex that derive from 2.65–2.60 Ga (mainly tonalites and granodiorites) (Rosa-Costa et al., 2003, 2006); (5) several plutons of charnockite, enderbite and mesoperthite-bearing granites dated at 2.65–2.60 Ga that have been grouped in the Noucouru Intrusive Suite (Ricci et al., 2002; Rosa-Costa et al., 2006); and (6) high- to medium-grade gneisses, with inferred Archaean ages and not included in any specific stratigraphic unit, are informally referred to as a granulitic–gneissic–migmatitic complex.

The Archaean basement of the Amapá Block records Palaeoproterozoic successive overprinting as indicated by the emplacement of several syn- to late-orogenic granitic plutons at about 2.22, 2.18, 2.15, 2.05 and 2.03 Ga. These granites have Nd isotope signatures suggesting reworking of Archaean crust (Rosa-Costa et al., 2003, 2006). Furthermore, U–Th–Pb dating of monazite from high-grade gneisses indicates that the granulite facies metamorphism took place at about 2.10–2.09 Ga, during the collisional stage of the Transamazonian orogenic cycle (Rosa-Costa et al., 2008). Monazite ages also reveal late-orogenic migmatization at about 2.06 and 2.04 Ga occurring under amphibolite facies conditions and coeval to the emplacement of granite plutons.

The Carecuru Domain is composed of calc-alkaline gneisses and granitoids of the Paru–Maratiá Complex and the Carecuru Intrusive Suite, respectively, which yielded zircon ages between 2.19 and 2.14 Ga (Rosa-Costa et al., 2006). These calc-alkaline units have T_{DM} model ages between 2.50 and 2.28 Ga, with ε_{Nd} values of +1.63 to −0.84, indicating the participation of juvenile, mantle-derived protoliths in addition to minor Archaean components in their source (Rosa-Costa et al., 2006). The granitoids are variably deformed, showing penetrative foliation to preserved igneous textures and the supracrustal rocks underwent greenschist to amphibolite facies metamorphism (Rosa-Costa et al., 2003, 2006). Supracrustal sequences of this domain consist of mafic and intermediate metavolcanic rocks grouped in the Fazendinha, Treze de Maio and Cuiapocu sequences. Metavolcanic and metasedimentary rocks, including banded iron formation, also made up the Ipitinga Group that defines the boundary between the Amapá Block and the Carecuru Domain (Rosa-Costa et al., 2003). A metavolcanic rock of this group yielded a whole-rock Sm–Nd isochron of 2267 ± 66 Ma (McReath and Faraco, 2006). Several granitic plutons, including syn-tectonic leucogranites, intruded the calc-alkaline gneisses and granitoids and the supracrustal belts. This magmatism represents syn- to late-orogenic crustal reworking occurring between 2.14 and 2.10 Ga (Rosa-Costa et al., 2006). In addition, small bodies of syn-tectonic muscovite- and/or garnet-bearing crustal granites were emplaced in strike–slip structures, close to limit between the Carecuru Domain and the Amapá Block (Fig. 1) at about 2.03 Ga (Rosa-Costa et al., 2006). The Carecuru Domain represents a granitoid-greenstone terrane developed in a magmatic arc setting that was accreted to the southwestern border of the Amapá Block during the Transamazonian orogenic cycle (Rosa-Costa et al., 2006).

Within the Carecuru Domain a granulitic nucleus, the Paru Domain, crops out and represents a basement inlier. This nucleus is composed of granulitic orthogneisses of the Ananaí Complex of 2.60 Ga in addition to Palaeoproterozoic charnockites and mesoperthite-granites of the Igarapé Urucu Intrusive Suite, dated at 2.16 to 2.07 Ga (Rosa-Costa et al., 2003). The youngest magmatic activity in the region is ascribed to the intrusion of anorogenic plutons of the Waiãpi Granite at about 1.75 Ga (Vasquez and Lafon, 2001).

3. Metamorphic and structural framework of the Ipitinga Auriferous District

Granulite facies metamorphism is widespread in the south-eastern Guiana Shield. In the granulitic Paru Domain that occurs within the Carecuru Domain, the intrusion of charnockites of 2074 ± 5 Ma (Igarapé Urucu Intrusive Suite; Fig. 1) has been considered as an indicator of the time of high-grade metamorphism in that inlier (Rosa-Costa et al., 2006 and references therein).

In the Ipitinga Auriferous District of the Carecuru Domain, the peak of metamorphism for the metavolcano-sedimentary Ipitinga Group that hosts the gold mineralisation at Carará has been estimated at 530 to 540 °C and 3 to 4 kbar (lower amphibolite facies), with retrogression to the greenschist facies at 250 to 450 °C and 0.7 to 2.3 kbar (Faraco et al., 2006). The timing of this metamorphic event has been constrained by U–Th–Pb dating of monazite from a calc-alkaline diorite of the Carecuru Intrusive Suite, which yielded an age of 2038 ± 6 Ma (Rosa-Costa et al., 2008).

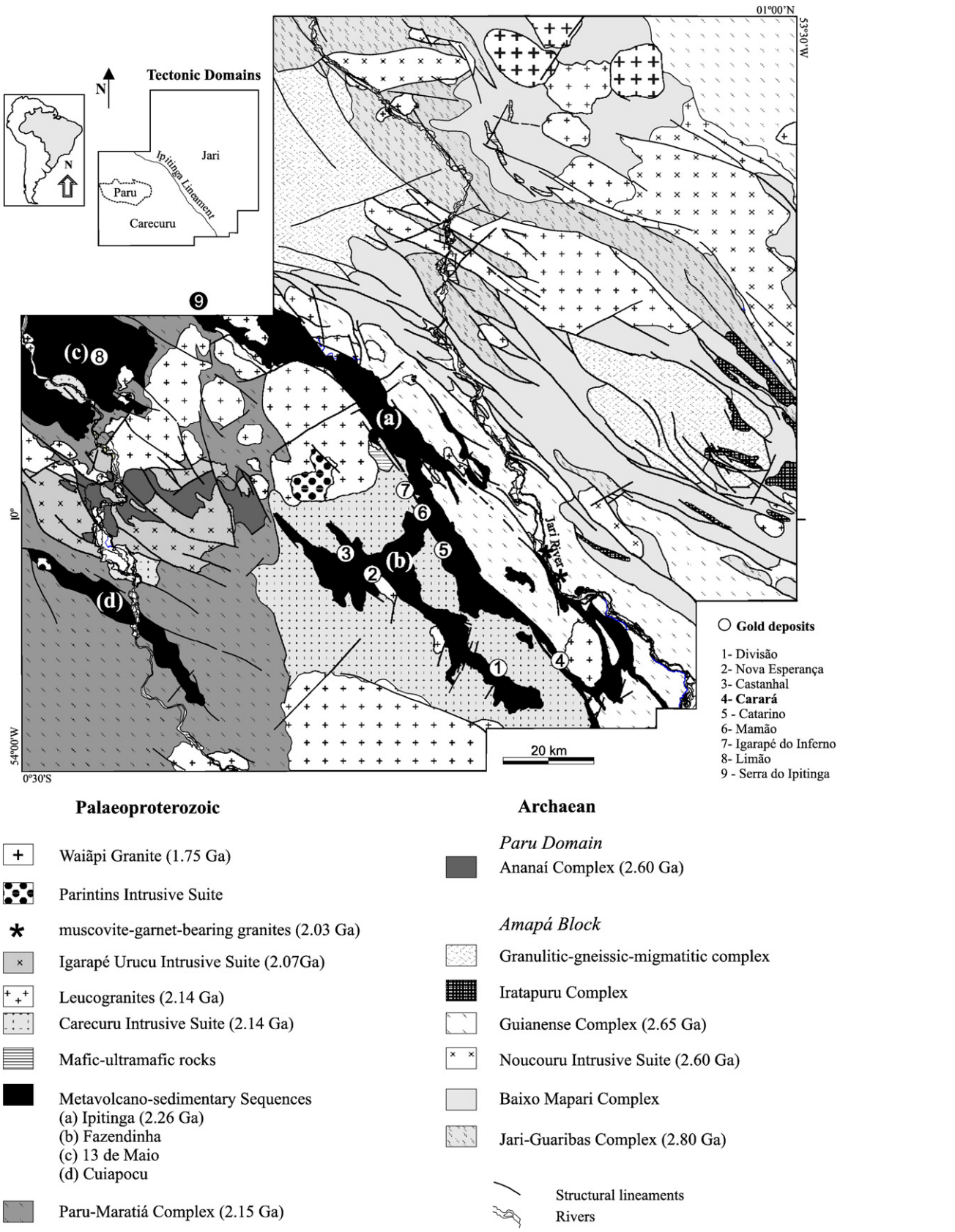

Fig. 1. Location map and geological map of the south-eastern portion of the Guiana Shield (modified from Rosa-Costa et al., 2006, 2009), with the location of gold deposits and showings of the Ipitinga Auriferous District.

The structural framework of the Ipitinga Auriferous District was described by Klein and Rosa-Costa (2003) and Rosa-Costa et al. (2003). It is mainly defined by a subvertical NW–SE-trending foliation (schistosity), characterized by the preferred orientation of mica, chlorite and amphibole grains, which is observed especially in the metavolcanic-sedimentary sequences and subordinately in the intrusive and broadly coeval

granitoids. The regional foliation is parallel to the major tectonic discontinuities. However, in places, it is parallel to the contacts between the supracrustal sequences and the granitoid plutons. This schistosity has overprinted primary structures (bedding) of the rocks, which are no longer recognized. A down dip to slightly oblique elongation lineation is contained in the foliation planes. Slickenline planes are also present, especially at the contact between veins and their host rocks. The schistosity is locally folded into open to recumbent folds. A strike–slip movement is evident especially along the boundary between the Carecuru Domain and the Amapá Block, overprinting early thrust structures and showing both dextral and sinistral kinematic features. However, in the inner portions of the supracrustal sequences, steep lineations dominate, suggesting limited strike–slip influence during the ductile deformation. These structural elements likely record a compressive deformation event, showing effects of NE–SW shortening (D1) followed by the transcurrent regime (D2). Second- and third-order structures are present as well, being both parallel and oblique to the strike of the first-order ones. These subsidiary structures are dominantly moderate to high-angle reverse to reverse-oblique in nature (Klein and Rosa-Costa, 2003). The strike–slip structures (D2) were active by 2030 ± 2 Ma, which is constrained by the intrusion of syn-tectonic muscovite- and/or garnet-bearing crustal granites (Fig. 1) (Rosa-Costa et al., 2006).

4. The Carará deposit

4.1. Local geology

Mineralisation in the Ipitinga Auriferous District is closely related to two sets of supracrustal sequences, the Ipitinga Group and the Fazendinha Sequence (Fig. 1). Mineralised structures in the district have been interpreted to be related to the evolution of the Ipitinga lineament (Klein and Rosa-Costa, 2003). The Carará gold deposit is located in the south-eastern portion of the Ipitinga Auriferous District and is hosted in a metasedimentary rock of the Ipitinga Group close to the tectonic limit between the Carecuru Domain and the Amapá Block. In the vicinities of the deposit the Ipitinga Group is tectonically juxtaposed to the Guianense Complex along the Ipitinga lineament. Both units have been intruded by the Carecuru Intrusive Suite and leucogranites (Fig. 1).

4.2. Deposit geology

The Carará deposit had been mined for several years until mine closure in the beginning of the 1990's. Geological resources of 10 tonnes Au have been determined (Carvalho et al., 1995) and gold grades in the vein and wall-rock vary significantly along the strike, from 2.72 to 53.42 g/t and 0.18 to 17.21 g/t, respectively (Fig. 2). A better understanding of the geological conditions around the deposit is hampered by the thick lateritic cover. Gold mineralisation is associated with a quartz vein and its 10 to 50 cm-thick hydrothermal halo. The wall-rock is a tourmaline- and muscovite-bearing quartzite with subordinate pyrite content (Fig. 3). The quartzite shows a NNW–SSE-striking schistosity that dips 75° to 85° to the SW. The schistosity is defined by the preferred orientation of muscovite crystals and is conformable to the regional foliation. The schistosity planes contain an elongation lineation that plunges at high angles in, or slightly oblique to, the dip direction (70°S/30°W).

The gold–quartz vein shows variable thickness, from 15 cm to 3 m (Figs. 2 and 4), and can be traced by more than 400 m along strike, and at least by 70 m in depth. The quartz vein occupies the central part of a shear zone, which is defined by large contents of muscovite and tourmaline close to the vein walls (Fig. 4A). Both muscovite and tourmaline grains define an elongation lineation that indicates reverse to slightly reverse-oblique movement along the vein, characterizing a high-angle reverse shear zone, and suggest that the shear zone was active at the time of vein formation. These features allow the quartz vein be classified as a central shear vein, according to Hodgson (1989). The vein shows massive to saccharoidal textures and the absence of laminated texture with fragments of the wall-rock inside the vein may suggest a single stage of dilation and hydrothermal sealing (e.g., Cox, 1995). In addition, saccharoidal texture indicates, at least moderate crustal levels (mesozonal) for vein emplacement.

Tourmaline forms well developed layers at the contact between the vein and the wall-rock (Fig. 4A), and two types can be observed. One type forms aggregates of small dark-green prismatic crystals. The other type is formed by larger and more limpid brownish crystals having less solid inclusions than the dark-green ones. Both types may occur in spatial association and both are associated with quartz. Muscovite occurs as small platy and oriented crystals, and sulphide minerals (pyrite) are

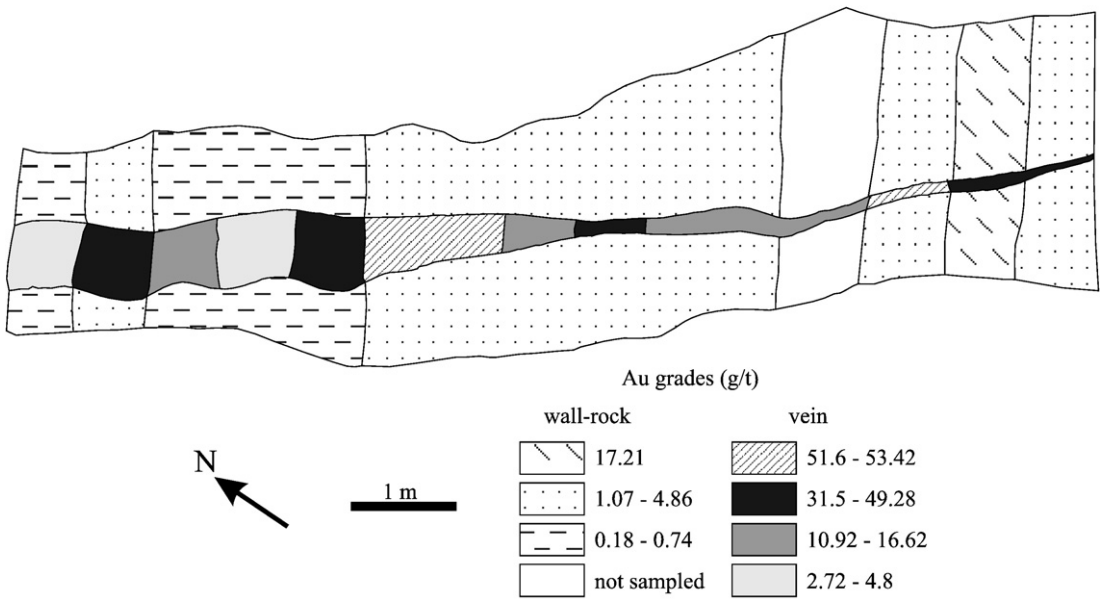

Fig. 2. Sketch map of level 70, shaft 3 of the Carará gold deposit showing the variation in gold grades along the quartz vein and host quartzite. The subdivisions are schematic and are based on 30 analyses.

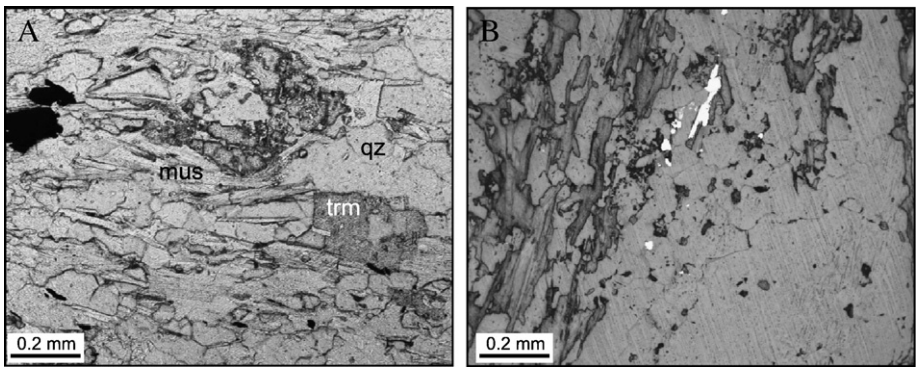

Fig. 3. Photomicrographs of the host rock at Carará. (A) Foliated quartzite composed of quartz (qz), muscovite (mus) and tourmaline (trm); (B) Deformed pyrite crystals (white) placed within the foliation of a muscovite-bearing (dark-grey) quartzite.

extremely rare and negligible. Networks of microfractures filled with quartz and/or muscovite and tourmaline crosscut both the quartz vein and the wall-rock and are the sites of gold deposition. Small quartz veinlets (<1 cm) cut the tourmaline-rich zone and are called here late barren quartz veinlets.

4.3. Timing of gold mineralisation

Geological information described in the previous section indicates that gold mineralisation in the Ipitinga Auriferous District is post-metamorphic and closely related to the development of the host strike–slip shear zones (Klein and Rosa-Costa, 2003; Klein et al., in press). Dating of hydrothermal muscovite from Carará and the nearby and similar Catarino occurrence, using the ^{40}Ar–^{39}Ar method, yielded ages of 1940 ± 20 Ma and 1930 ± 20 Ma, respectively (Klein et al., in press). These ages are similar to biotite ages of 1928 ± 9 Ma and 1833 ± 13 Ma reported by Rosa-Costa et al. (2009), which have been interpreted as reflecting post-crystallization isotopic resetting induced by a widespread thermal event associated with the emplacement of anorogenic granitoids elsewhere in the Amazonian Craton at 1.88 to 1.86 Ga, and the emplacement of the Waiãpi Granite at 1.75 Ga in the south-eastern Guyana Shield. Accordingly, the ^{40}Ar–^{39}Ar isotopes constrain only minimum ages for gold mineralisation at Carará and elsewhere in the Ipitinga Auriferous District, which is then bracketed between 2030 and 1940 Ma. Given the synchronicity between veining and deformation at Carará, mineralisation in this deposit likely occurred at about 2030 Ma.

4.4. Summary of published stable isotope data

Klein et al. (in press) conducted a reconnaissance stable isotope study in vein materials from the Carará deposit, in order to trace possible sources for the ore-bearing fluid. At a temperature of 346 °C, and using the fractionation factors of Kotzer et al. (1993) and Chacko et al. (1996), the $\delta^{18}O_{H2O}$ values calculated from quartz range from +6.4 to +7.0‰ in the mineralised veins, and from +5.2 to +5.6‰ in the late barren quartz veinlet. Values calculated from tourmaline and muscovite lie in the range between +7.0 and +8.3‰. The δD_{H2O} values of inclusion fluids are −33‰ in the low-grade quartz and −61‰ in the late barren quartz veinlets; values calculated from hydrous silicates vary between −20 and −34‰. The oxygen isotope values for the fluid lie within the range for both metamorphic and magmatic sources. However, combined oxygen and hydrogen values consistently indicate a metamorphic source for the water in the mineralised veins at Carará. The fluid composition for the late barren quartz veinlets, which is clearly distinct from that of mineralised quartz, probably reflects a magmatic source.

The measured $\delta^{13}C$ values of carbon CO_2 in fluid inclusions are −3.4‰, −3.2‰, and −14.6‰ in the high-grade, low-grade, and late barren quartz veins, respectively (Klein et al., in press).

5. Sampling and analytical procedures

Samples have been collected on surface mined exposures of the deposit. Studies were undertaken in different portions of the vein-quartz (Fig. 4), here referred to as high-grade quartz, low-grade quartz, and late barren quartz veinlet. Petrographic, microthermometric and Raman spectroscopic studies were conducted on fluid inclusions hosted in quartz crystals of the three vein/zones. Doubly-polished thick sections were examined under the petrographic microscope prior to the heating and freezing experiments to record the distribution, size, types, and textural relationships of the fluid inclusions. The microthermometric study was carried out at the Universidade Federal do Pará (Belém, Brazil) using a Chaixmeca heating–freezing stage and following procedures described elsewhere (Roedder, 1984; Shepherd et al., 1985; Wilkinson, 2001). The equipment was previously calibrated with synthetic samples of fluid inclusions. The data are reproducible to ±0.5 °C for the freezing runs down to −180 °C and ±5 °C for the heating runs up to the appropriate temperature of total homogenisation. About 250 fluid inclusions have been investigated by microthermometry in this study.

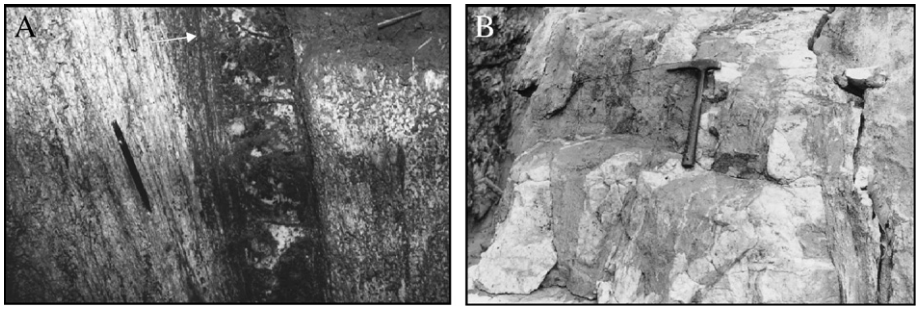

Fig. 4. Photographs of the (A) high-grade quartz vein with high concentration of tourmaline (white arrow) in the contact with the host rock (the pen is 14 cm long), and (B) low-grade quartz vein. In both cases the host rock is a quartzite.

Raman spectrographic studies were carried out at the Universidade Federal de Minas Gerais (Belo Horizonte, Brazil), with a laser-excited Dilor multichannel microprobe, using the 514.53 nm line of an argon laser. Integration time was 10 s with ten accumulations for each spectral line, and calibration was made with mercury light.

6. Fluid inclusions

6.1. Petrography, distribution and types

Both high- and low-grade quartz show saccharoidal texture, with large, rounded to irregularly shaped crystals cemented by a mass of fine-grained quartz grains (Fig. 5). The larger grains show undulose extinction and minor subgrain development. In the late quartz veinlets, quartz forms aggregates of medium-grained crystals with serrated contacts (Fig. 5E). Many crystals are strain-free, recrystallized grains, lacking fluid inclusions.

The distribution of the fluid inclusions is similar in the three types of quartz. They occur dominantly along narrow to large transgranular and intragranular trails that terminate against grain boundaries or within individual crystals (Fig. 5). Isolated inclusions and clusters of randomly distributed inclusions are also frequent. Some grains show clouds or swarms of tightly-spaced subparallel trails of fluid inclusions. These textural relationships show that the inclusions cannot all be defined as primary inclusions, in the sense of Roedder (1984).

Two different types of fluid inclusions have been identified based on the number of phases and liquid to vapour ratios at room temperature (Fig. 5). Type 1 consists of one-phase vapour-rich fluid inclusions that occur in the three types of quartz and is the unique type present in the high- and low-grade quartz samples. The inclusions of this type are generally dark, with negative crystal morphologies, mostly varying in size between 5 and 15 μm.

Type 2 comprises two-phase, liquid-rich fluid inclusions that are restricted to the late quartz veinlet. Only seven measurable (>5 μm) fluid inclusions belonging to this type have been recognized occurring in two clusters in association with the Type 1. They consist of a dark gaseous bubble and a clear liquid phase, with a rather constant gas/liquid ratio of 0.25 to 0.40. Under cooling, a new bubble nucleated in both types 1 and 2 fluid inclusions, allowing them to be defined as carbonic and aqueous-carbonic inclusions, respectively.

6.2. Microthermometric and micro-Raman results

During the microthermometric work several runs have been undertaken down to the lowest limit of temperature of the heating–freezing stage (~180 °C), in order to detect the presence of CH_4 and/or N_2. However, all inclusions froze between −100 and −120 °C, indicating that these compounds are not present in significant amounts.

After heating from these low temperatures, the melting of CO_2 (T_mCO_2) in both carbonic and aqueous-carbonic types occurred in a relatively narrow interval, in all types of quartz, between −56.6 and −58.2 °C, with a sharp peak being observed at −57.4 °C (Fig. 6A), indicating the dominance of CO_2 and the presence of other gases in subordinate amounts. In fact, micro-Raman spectroscopic analysis of a few fluid inclusions identified only traces of CH_4 and C_2H_6 (ethane) and up to 2 mol.% of N_2 in inclusions from the high-grade quartz.

Homogenisation of the carbonic phase (T_hCO_2) of the type 1 inclusions occurred to liquid in a wide range of temperatures, from −28.5 to +29.9 °C, with most of the values clustering between +2 and +10 °C.

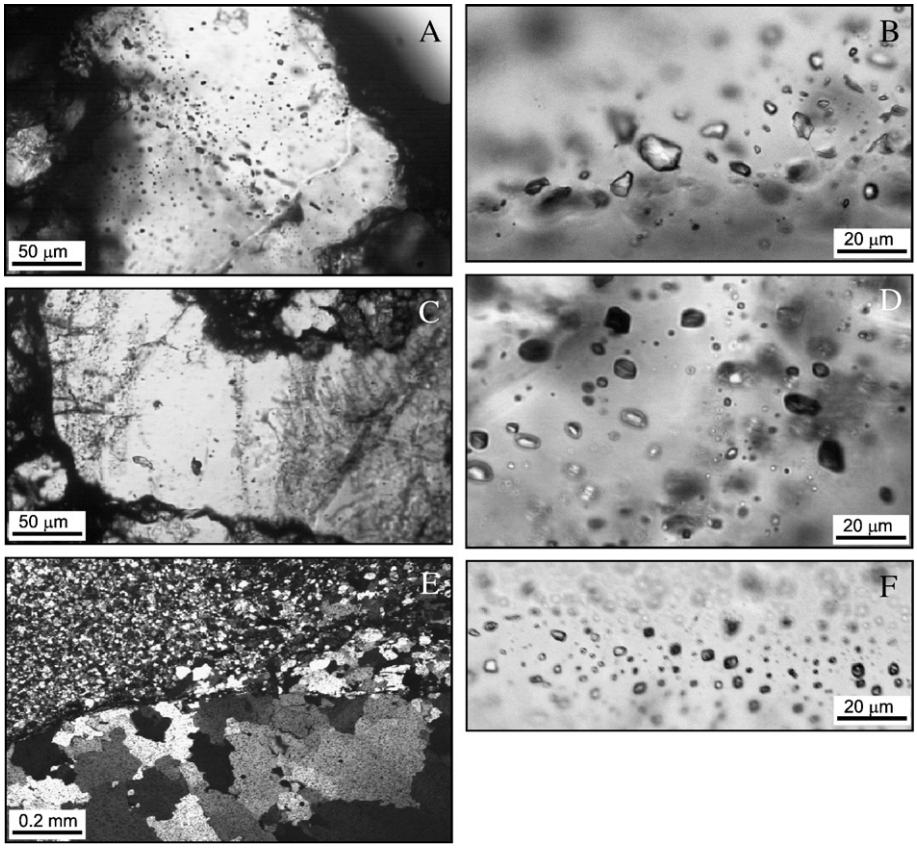

Fig. 5. Photomicrographs showing types and distribution of fluid inclusions in veins from the Carará gold deposit. (A) Quartz crystal of the high-grade quartz vein with clouds and trails of one-phase carbonic fluid inclusions. (B) Detail of photograph A, showing a planar array of carbonic inclusions with negative crystal shape. (C) Quartz crystal of the low-grade quartz vein with trails of one-phase carbonic inclusions. (D) Detail of photograph C showing planar arrays of carbonic inclusions with negative crystal shape. (E) Barren late quartz veinlet crosscutting the host rock. (F) Detail of photograph E showing a trail with a few two-phase aqueous-carbonic inclusions.

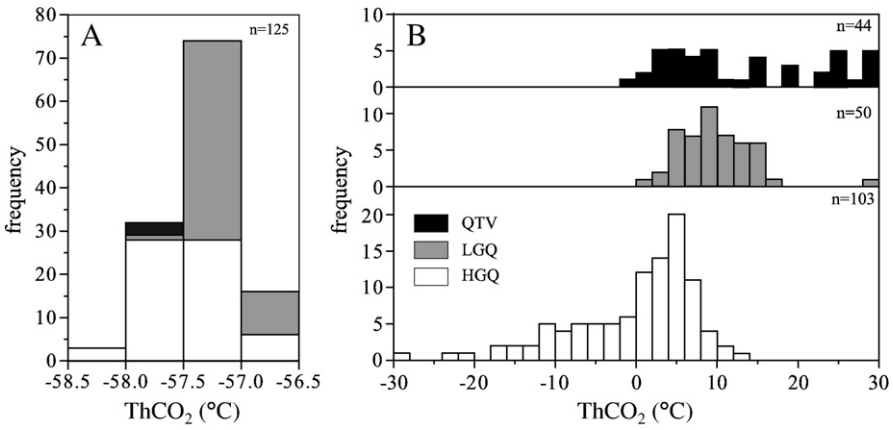

Fig. 6. Frequency histograms showing the microthermometric properties of fluid inclusions from the Carará gold deposit. (A) Melting temperature of the carbonic phase (T_mCO_2). (B) Homogenisation temperature of the carbonic phase (T_hCO_2) for individual types of quartz veins. LGQ (low-grade quartz), HGQ (high-grade quartz), QTV (late barren quartz quartz-tourmaline veinlet).

However, the distribution of values varies among distinct samples (Fig. 6B). In the high-grade quartz only temperatures below 12.9 °C have been recorded (corresponding to high CO_2 densities of 1.070 to 0.893 g/cm^3), and internal variations in a single cluster or trail of this vein are mostly of 2 to 7 °C, although variations can reach as much as 30 °C. Furthermore, all moderate to strongly negative temperatures have been recorded only in this type of quartz and the shape of the histogram is strongly skewed to the right.

In the low-grade quartz T_hCO_2 varied between 0 and 18 °C (CO_2 densities of 0.928 to 0.795 g/cm^3), with the histogram showing a poorly defined peak at 9 °C (Fig. 6B). In the late quartz veinlets, the homogenisation ranges from −0.3 to 29.9 °C (densities of 0.930 to 0.600 g/cm^3), and the values are discontinuously distributed (Fig. 6B).

Formation of clathrates was not observed in Type 1 inclusions, which was expected given the absence of visible water in the inclusions. Surprisingly, however, H_2O that was not identified in the petrographic and microthermometric studies was detected by the Raman analysis in some inclusions. This compound is, thus, subordinate (<10 vol.%) and likely occurs as tiny "invisible" rims involving the CO_2 bubble (e.g., Hedenquist and Henley, 1985).

In the seven Type 2 aqueous-carbonic fluid inclusions from the late quartz veinlet, $TmCO_2$ values were recorded mostly at −57.7 °C, but also at −56.6 °C. The T_hCO_2 took place to liquid between 23.5 and 26.5 °C (densities of 0.70–0.73 g/cm^3), and clathrates melted between 7.2 and 7.6 °C, indicating salinities around 5.0 to 5.4 wt.% NaCl equiv.. The final homogenisation, also to liquid, occurred in the range of 264 to 346 °C.

7. Discussion

7.1. Origin of the one-phase carbonic fluid inclusions

The peculiar absence of significant H_2O contents in the fluid inclusions contrasts with the hydrous mineralogy (muscovite + tourmaline) occurring in close association with the gold–quartz vein. This might be product of: (1) preferential leakage of H_2O from the inclusions; (2) unmixing of a H_2O–CO_2 fluid followed by preferential trapping of CO_2; and/or (3) two fluids (CO_2-rich and H_2O-rich) operating separately.

Water leakage leads to a decrease in the density of the remaining fluid (Crawford and Hollister, 1986; Huizenga and Touret, 1999; Klein et al., 2006). However, the inclusions in the high-grade quartz show the highest density values. Furthermore, other textural evidence of leakage, such as tiny trails of aqueous inclusions departing from the larger carbonic inclusions, is also lacking. Moreover, T_hCO_2 variations in micro-domains of the host quartz are in general limited. So, it is unlikely that their water content has significantly leaked, and the dense CO_2-rich fluid inclusions may probably represent the closest relics of the original fluid.

Unmixing of an aqueous-carbonic fluid at or near the solvus and at the depositional site is ruled out, since it must be texturally demonstrated by heterogeneous trapping, i.e., the presence of cogenetic aqueous and/or aqueous-carbonic fluid inclusions (e.g., Ramboz et al., 1982). Unmixing before trapping could be facilitated by the physical separation of the immiscible phases due to the density contrast and differences in the wetting properties between CO_2 and H_2O (Watson and Brenan, 1987) during grain boundary migration deformation (Johnson and Hollister, 1995). Even in this case, however, the presence of aqueous inclusions, especially decorating grain boundaries, would be expected as well (Crawford and Hollister, 1986; Johnson and Hollister, 1995).

Unmixing is still a valid hypothesis if it has occurred well before trapping, outside the depositional site, and the aqueous and the carbonic phases were isolated by the mechanism described above. In this case, the original fluid should be CO_2-dominated, which is not the rule in orogenic gold deposits. In a detailed discussion conducted by Chi et al. (2009) concerning the Campbell-Red Lake deposit, Canada, simulating different *P*–*T* conditions and proportions of CO_2 and H_2O for the pre-unmixing fluid, the authors concluded that unmixing could produce the carbonic fluid from an original fluid with $XCO_2 > 0.8$.

Therefore, phase separation of a CO_2-rich, H_2O-poor fluid well before trapping with subsequent physical isolation of the two phases and the existence of two fluids, carbonic and aqueous, operating separately are the best possible explanations for the origin of the carbonic inclusions at Carará. Based only in the data we discussed here, there is no element to favour either of the two models. The important fact here, however, is the recognition of a CO_2-dominated parental fluid. Regardless of the chosen model, the CO_2 phase has been trapped in fluid inclusions in the veins whereas the aqueous phase has been consumed to produce the muscovite-tourmaline alteration in the vein–host rock contact.

7.2. Source of CO_2 and C_2H_6

At Carará, the variation in the composition of the carbonic fluid in the two types of mineralised veins (high- and low-grade quartz), given by the T_mCO_2 and $\delta^{13}C_{CO2}$ values, is negligible, indicating that the same fluid has been trapped in these veins. These values, combined with the high CO_2 density, indicate deep-seated sources (mantle, metamorphic or magmatic) for this carbon and rule out marine and organic contributions. We propose that the voluminous charnockite magmatism and/or the coeval granulite facies metamorphism are possible sources of the CO_2 at Carará. Felsic magmas emplaced at depth and metamorphism of the hosting supracrustal sequences are alternative explanations. The $\delta^{13}C_{CO2}$

value of the late barren quartz veinlet is rather different. The source of this lighter carbon remains unknown, but contribution of organic carbon in shallower levels of the crust is a possible explanation.

The presence of C_2H_6 and other light hydrocarbons in fluid inclusions from gold–quartz vein deposits has been documented in a few cases in the Canadian Abitibi belt (Graney and Kesler, 1995), in the Barberton greenstone belt of South Africa (Bray et al., 1991; De Ronde et al., 1992), and in the Yilgarn block of Western Australia (Polito et al., 2001). In the latter case, the source of these hydrocarbons appears to be a reduction of CO_2 to CH_4 and C_2H_6.

7.3. Trapping conditions

Despite the similar composition within the mineralised veins, differences in the evolution and/or trapping conditions of the carbonic fluid at Carará are indicated by large variations in T_hCO_2 (Fig. 6B), i.e., in the density of the carbonic fluid. This large density range may be explained by different processes that include trapping of fluids with decreasing density; trapping of fluid under fluctuating fluid pressure; re-equilibration under retrogressive conditions during uplift; water leakage or a combination of these.

The statistical evaluation of microthermometric data shows that, at least for the high-grade quartz, the global variation in T_hCO_2 values (−28.5 to 12.9 °C), the moderate standard deviation (7.5 °C), the absence of correlation between inclusion size and T_hCO_2 (Fig. 7A), and the shape of the histogram, skewed to the right (Fig. 6B), strongly indicate density re-equilibration during deformation under plastic regime, at high temperature and low strain rate, according to the criteria of Vityk and Bodnar (1998). In this case, the average T_hCO_2 (−0.5 °C) represents the internal overpressure that could have been maintained for most of the re-equilibrated fluid inclusions (Fig. 8). Furthermore, the isochore that represents the average T_hCO_2 is compatible with the geothermal gradient inferred for the area (Fig. 8). Moreover, the inclusions showing the highest densities likely represent the closest composition of the parental deeply-sourced fluid. The low-grade quartz appears to have trapped only the re-equilibrated fluid, because the isochore of highest density of this quartz equals the isochore of average T_hCO_2 of the high-grade quartz. In addition, the positive correlation between inclusion size and T_hCO_2 (Fig. 7B) and the poorly defined multimodal histogram (Fig. 6B) may indicate brittle deformation (Touret, 1994; Vityk and Bodnar, 1998).

For the two-phase aqueous-carbonic fluid inclusions of the late barren quartz veinlet, the homogenisation temperatures vary between 264 and 346 °C. Isochores calculated for these inclusions intercept the solvus of the CO_2–H_2O–NaCl chemical system at 280 to 286 °C and 1.6 to 2.0 kbar (Fig. 8). These are considered minimum (or final) trapping conditions for the mineralised veins. Klein et al. (in press) reported temperatures of 475 and 447 °C for Carará and the nearby (and geologically similar) Catarino showing, respectively, based on oxygen isotope fractionation between hydrothermal quartz and muscovite. These temperatures lie close to the upper limit of the retrogressive, greenschist facies metamorphic event established by Faraco et al. (2006) and likely represent the conditions of the hydrous alteration.

It is, however, likely that a hot, high density CO_2-rich fluid started to be trapped at amphibolite facies or higher conditions and became progressively re-equilibrated under retrogressive conditions. The main entrapment occurred at conditions that surround the average isochore and a *P–T* window (Fig. 8) may be limited by the intersection of the maximum homogenisation temperature of the aqueous-carbonic fluid inclusions of the late quartz-tourmaline veinlet and the temperature yielded by the quartz–muscovite pair with the lowest isochore of the high-grade quartz fluid inclusions and the geothermal gradient. This implies 350 to 475 °C, 1.8 to 3.6 kbar and 7 to 12 km depth for vein formation, hydrothermal alteration and gold mineralisation. The isochore of the highest density approximates the parental fluid conditions and the large pressure variation is consistent with the active structural environment described for the deposit.

7.4. The role of CO_2 in ore formation

Despite the ubiquitous association of CO_2 with hydrothermal ore deposits, little is known about the role of CO_2 as a ligand or its direct participation in ore formation. Few studies provide any indication of metal mobilization by this volatile (e.g., Higgins, 1980; Keppler and Wyllie, 1990). The main arguments used against an original CO_2-rich fluid and a direct role in gold transport are: (1) wall-rock alteration, generally enriched in hydrous phases, requires the presence of an aqueous fluid; (2) the limited solubility of CO_2 in silicate melts (e.g., Walther and Orville, 1983); (3) the scarcity of constraints on the solubility of metals in CO_2 (Ridley and Diamond, 2000); (4) the weak chemical bonding between gold ions and CO_2 species (Phillips and Evans, 2004); and (5) the more accepted transport of gold as hydrosulphide or chloride complexes, instead of by a CO_2-rich fluid (e.g., Romberger, 1990; Seward, 1991). Lowenstern (2001) stressed that a possible explanation for this discrepant behaviour is that CO_2 is a very common gas in magmatic and other hydrothermal systems and, thus, it should be ubiquitous.

Possibly, CO_2 plays an indirect role in gold transport. For instance, CO_2 facilitates unmixing and creation of a separate vapour phase, which, in turn, might move sulphur and chlorine species to the vapour and act as ligands for metals. At the same time, phase separation will change other physico-chemical properties of the fluid, such as PCO_2 and pH, causing destabilization of metal-transporting complexes and, consequently, ore precipitation. Therefore, CO_2 would act at least on the creation and evolution of metal-bearing vapours (Lowenstern, 2001). Furthermore, Phillips and Evans (2004) proposed that CO_2, as a weak acid, might help gold transport by buffering the fluid in a pH range where high gold

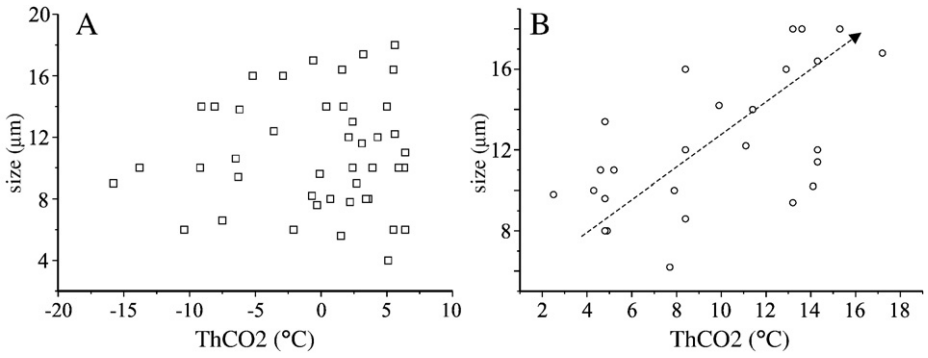

Fig. 7. Diagrams showing the relationships between homogenisation temperature (T_hCO_2) and inclusion size for fluid inclusions from the high-grade quartz (A) and low-grade quartz (B). The dashed arrow in B indicates the positive correlation between the compared properties.

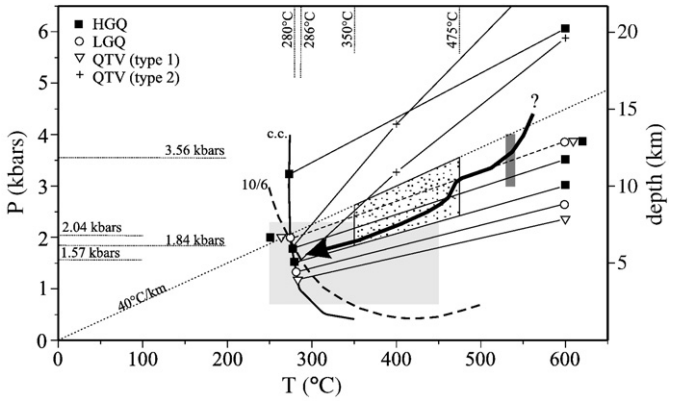

Fig. 8. *P–T* diagram showing isochores calculated for fluid inclusions in the different vein types of the Carará gold deposit: LGQ (low-grade quartz), HGQ (high-grade quartz), QTV (late barren quartz quartz-tourmaline veinlet). Types 1 and 2 are one-phase carbonic and two-phase aqueous-carbonic fluid inclusions, respectively. The dashed curve labelled 10/6 represents the solvus for the CO_2–H_2O–NaCl system with XCO_2 of 10 mol.% and 6 wt.% NaCl equiv. The thick solid line labelled c.c. is the critical curve for H_2O–CO_2 (both curves are from Bowers and Helgeson, 1983). The dotted line represents the geothermal gradient assuming lithostatic overburden. The dark and light grey shaded areas represent the peak and retrogressive metamorphic conditions, respectively, for the hosting sequence, as determined by Faraco et al. (2006). The stippled area defines the estimated predominant *P–T* conditions for the entrapment of the CO_2-rich fluid and the arrowed line represents the possible *P–T* path followed by the CO_2 fluid.

concentration could be maintained by reduced sulphur complexes. Moreover, studies of Lai and Chi (2007) suggest that CO_2-rich vapour is capable of transporting large amounts of Cu, and possibly Au.

8. Conclusions

The petrographic, microthermometric and micro-Raman study of the peculiar assemblage of CO_2-rich fluid inclusions with no visible water sampled from the Au–quartz vein of the Carará deposit, integrated with regional geological information and available isotopic data allow the following observations and conclusions:

(1) Primary and pseudo-secondary CO_2-rich fluid inclusions display variable densities that reflect re-equilibration during and after trapping.
(2) The densest (>0.9 g/cm^3) inclusions approximate the conditions of the parental fluid. This parental fluid may be either an originally CO_2-rich fluid or a fluid produced by phase separation of an carbonic-aqueous fluid having $XCO_2 > 0.8$.
(3) The CO_2 fluid was channelled in fractures and trapped in veins, whereas an H_2O-rich fluid provoked the hydrous alteration around the vein.
(4) Most fluid inclusions were trapped and/or re-equilibrated at 350 to 475 °C and 1.8 to 3.6 kbar, which implies 7 to 12 km of depth for vein formation. Trapping, however, commenced earlier, at least in the amphibolite facies conditions.
(5) The potential deep-seated sources for the CO_2 fluid are the 2074 Ma old charnockites and/or the coeval granulite facies metamorphism.
(6) The role of CO_2, whether capable of transporting gold complexes or, alternatively, as an agent to provide adequate physico-chemical conditions for gold transport and deposition, is not yet understood.

Acknowledgements

Field work was done during the RENCA Project developed by CPRM/Geological Survey of Brazil. The authors thank the thoughtful comments of two OGR anonymous reviewers. The senior author acknowledges the Brazilian *Conselho Nacional de Desenvolvimento Científico e Tecnológico* (CNPq) for research grant 306994/2006-0.

References

Baker, T., 2002. Emplacement depth and carbon dioxide-rich fluid inclusions in intrusion-related gold deposits. Economic Geology 97, 1111–1117.
Bakker, R.J., Jansen, B.H., 1991. Experimental post-entrapment water loss from synthetic CO2–H2O inclusions in natural quartz. Geochimica et Cosmochimica Acta 55, 2215–2230.
Bowers, T.S., Helgeson, H.C., 1983. Calculation of the thermodynamic and geochemical consequences of nonideal mixing in the system H_2O–CO_2–NaCl on phase relations in geological systems: equation of state for H_2O–CO_2–NaCl fluids at high pressures and temperatures. Geochimica et Cosmochimica Acta 47, 1247–1275.
Bray, C.J., Spooner, E.T.C., Thomas, A.V., 1991. Fluid inclusion volatile analysis by heated crushing, on-line gas chromatography: application to Archaean fluids. Journal of Geochemical Exploration 42, 167–192.
Carvalho, J.M.A., Faraco, M.T.L., Klein, E.L., 1995. Metallogenic-Geochemical Map of Gold in Amapá and NW Pará States, Scale 1:500, 000: Explanatory Note. CPRM, Belém. 5 pp.
Chacko, T., Hu, X., Mayeda, T.K., Clayton, R.N., Goldsmith, J.R., 1996. Oxygen isotope fractionations in muscovite, phlogopite, and rutile. Geochimica et Cosmochimica Acta 60, 2595–2608.
Chi, G., Liu, Y., Dubé, B., 2009. Relationship between CO_2-dominated fluids, hydrothermal alterations and gold mineralization in the Red Lake greenstone belt, Canada. Applied Geochemistry 24, 504–516.
Cox, S.F., 1995. Faulting processes at high fluid pressures: an example of fault valve behavior from the Wattle Gully Fault, Victoria, Australia. Journal of Geophysical Research 100 (B7), 12841–12859.
Crawford, M.L., Hollister, L.S., 1986. Metamorphic fluids: the evidence from fluid inclusions. In: Walther, J.V., Wood, B.J. (Eds.), Fluid Rock Interaction During Metamorphism. Physical Geochemistry, vol. 5. Springer, New York, pp. 1–35.
De Ronde, C.E.J., Spooner, E.T.C., De Witt, M.J., Bray, C.J., 1992. Shear zone-related, Au quartz vein deposits in the Barberton Greenstone Belt, South Africa: field and petrographic characteristics, fluid properties, and light stable isotope geochemistry. Economic Geology 87, 366–402.
Faraco, M.T.L., Fuzikawa, K., Ramboz, C., McReath, I., 2006. A fluid inclusion study in the hydrothermal volcanogenic sulfide and orogenic gold mineralization at the Serra do Ipitinga, Amazon, Brazil. Revista Brasileira de Geociências 36 (suppl. 1), 51–58.
Garba, I., Akande, S.O., 1992. The origin and significance of non-aqueous CO_2 fluid inclusions in the auriferous veins of Bin Yauri, northwestern Nigeria. Mineralium Deposita 27, 249–255.
Graney, J.R., Kesler, S.E., 1995. Gas composition of fluid in ore deposits: is there a relation to magmas? In: Thompson, J.F.H. (Ed.), Magmas, Fluids and Ore Deposits. : Short Course Series, vol. 23. Mineralogical Association of Canada, pp. 221–245.
Hedenquist, J.W., Henley, R.W., 1985. The importance of CO_2 on freezing point measurements of fluid inclusions: evidence from active geothermal systems and implications for epithermal ore deposition. Economic Geology 80, 1379–1406.
Higgins, N.C., 1980. Fluid inclusion evidence for the transport of carbonate complexes in hydrothermal solutions. Canadian Journal of Earth Sciences 17, 823–830.
Ho, S.E., 1987. Fluid inclusions: their potential as an exploration tool for Archaean gold deposits. In: Ho, S.E., Groves, D.I. (Eds.), Recent Advances in Understanding Precambrian Gold Deposits. : Publication, vol. 11. Geology Department and University Extension, University of Western Australia, pp. 239–264.
Hodgson, C.J., 1989. The structure of shear-related, vein-type gold deposits: a review. Ore Geology Reviews 4, 231–273.
Hollister, L.S., 1990. Enrichment of CO_2 in fluid inclusions in quartz by removal of H_2O during crystal–plastic deformation. Journal of Structural Geology 12, 895–901.
Huizenga, J.M., Touret, J.L.R., 1999. Fluid inclusions in shear zones, the case of the Umwindsi shear zone in the Harare–Shamva–Bindura greenstone belt, NE Zimbabwe. European Journal of Mineralogy 11, 1079–1090.
Johnson, E.L., Hollister, L.S., 1995. Syndeformational fluid trapping in quartz: determining the pressure–temperature conditions of deformation from fluid inclusions and the formation of pure CO_2 fluid inclusions during grain-boundary migration. Journal of Metamorphic Geology 13, 239–249.
Keppler, H., Wyllie, P.J., 1990. Role of fluids in transport and fractionation of uranium and thorium in magmatic processes. Nature 348, 531–533.
Kerrick, D.M., Caldera, K., 1998. Metamorphic CO_2 degassing from orogenic belts. Chemical Geology 145, 213–232.
Klein, E.L., Rosa-Costa, L.T.R., 2003. Geology of quartz–vein gold deposits in the Ipitinga Auriferous District, northern Brazil, southeastern Guiana Shield. Géologie de la France 2-3-4, 231–242.
Klein, E.L., Harris, C., Renac, C., Giret, A., Moura, C.A.V., Fuzikawa, K., 2006. Fluid inclusion and stable isotope (O, H, C, and S) constraints on the genesis of the Serrinha gold deposit, Gurupi Belt, Northern Brazil. Mineralium Deposita 41, 160–178.
Klein, E.L., Lafon, J.M., Harris, C., Brito, R.S.C., Vaconcelos, P., in press. Fluid inclusion and isotopic constraints on the genesis of vein-quartz gold deposits of the Ipitinga Auriferous District, SE-Guiana Shield, Brazil. In: Rizzotto, G.J., Quadros, M.L.E.S. (Eds.), Contribuições à Geologia da Amazônia, vol. 6. Sociedade Brasileira de Geologia-Núcleo Norte, Belém.
Klemd, R., Hirdes, W., 1997. Origin of an unusual fluid composition in Early Proterozoic Palaeoplacer and lode-gold deposits in Birimian greenstone terranes of West Africa. South African Journal of Geology 100, 405–414.
Kolb, J., Kisters, A.F.M., Hoernes, S., Meyer, F.M., 2000. The origin of fluids and nature of fluid–rock interaction in mid-crustal auriferous mylonites of the Renco mine, southern Zimbabwe. Mineralium Deposita 35, 109–125.

Kotzer, T.G., Kyser, T.K., King, R.W., Kerrich, R., 1993. An empirical oxygen- and hydrogen-isotope geothermometer for quartz-tourmaline and tourmaline-water. Geochimica et Cosmochimica Acta 57, 3421–3426.

Lai, J., Chi, G., 2007. CO_2-rich fluid inclusions with chalcopyrite daughter mineral from the Fenghuangshan Cu–Fe–Au deposit, China: implications for metal transport in vapour. Mineralium Deposita 42, 293–299.

Lowenstern, J.B., 2001. Carbon dioxide in magmas and implications for hydrothermal systems. Mineralium Deposita 36, 490–502.

McReath, I., Faraco, M.T.L., 2006. Palaeoproterozoic greenstone-granite belts in Northern Brazil and the former Guyana Shield — West African Craton Province. Geologia USP Série Científica 5, 49–63.

Phillips, G.N., Evans, K.A., 2004. Role of CO_2 in the formation of gold deposits. Nature 429, 860–863.

Phillips, G.N., Powell, R., 1993. Link between gold provinces. Economic Geology 88, 1084–1098.

Polito, P.A., Bone, Y., Clarke, J.D.A., Mernagh, T.P., 2001. Compositional zoning of fluid inclusions in the Archaean Junction gold deposit, Western Australia: a process of fluid-wall–rock interaction? Australian Journal of Earth Sciences 48, 833–855.

Ramboz, C., Pichavant, M., Weisbrod, A., 1982. Fluid immiscibility in natural processes: Use and misuse of fluid inclusion data. II. Interpretation of fluid inclusion data in terms of immiscibility. Chemical Geology 37, 29–48.

Ricci, P.S.F., Carvalho, J.M.A., Rosa-Costa, L.T., Lafon, J.M., 2002. Plúton charnoenderbítico Arqueano intrusivo nos ortognaisses granulíticos do Cinturão Jari — Terreno Arqueano expressivo do sudeste do Escudo das Guianas. Congresso Brasileiro de Geologia. : Abstract Volume, vol. 41. Sociedade Brasileira de Geologia, pp. 524.

Ridley, J.R., Diamond, L.W., 2000. Fluid chemistry of orogenic lode gold deposits and implications for genetic models. Reviews in Economic Geology 13, 141–162.

Roedder, E., 1984. Fluid inclusions. Reviews in Mineralogy 12, 644 pp.

Romberger, S.B., 1990. Transport and deposition of gold in hydrothermal systems. In: Robert, F., Shearan, P.A., Green, S.B. (Eds.), Greenstone Gold and Crustal Evolution. : NUNA Conference Volume. Geological Association of Canada, pp. 61–66.

Rosa-Costa, L.T., Ricci, P.S.F., Lafon, J.M., Vasquez, M.L., Carvalho, J.M.A., Klein, E.L., Macambira, E.M.B., 2003. Geology and geochronology of Archean and Palaeoproterozoic domains of the southeastern Amapá and northwestern Pará, Brazil — southeastern Guyana shield. Géologie de la France 2-3-4, 101–120.

Rosa-Costa, L.T., Lafon, J.M., Delor, C., 2006. Zircon geochronology and Sm–Nd isotopic study: further constraints for the Archean and Palaeoproterozoic geodynamical evolution of the southeastern Guiana Shield, north of Amazonian Craton, Brazil. Gondwana Research 10, 277–300.

Rosa-Costa, L.T., Lafon, J.M., Cocherie, A., Delor, C., 2008. Electron microprobe U–Th–Pb monazite dating of the Transamazonian high-grade metamorphic overprint on Archean rocks from Amapá Block, southeastern Guiana Shield, northern Brazil. Journal of South American Earth Sciences 26, 445–462.

Rosa-Costa, L.T., Monié, P., Lafon, J.M., Arnaud, N.O., 2009. ^{40}Ar–^{39}Ar geochronology across Archean and Palaeoproterozoic terranes from southeastern Guiana Shield (north of Amazonian Craton, Brazil): evidence for contrasting cooling histories. Journal of South American Earth Sciences 27, 113–128.

Santosh, M., Jackson, D.H., Harris, N.B.W., Mattey, D.P., 1991. Carbonic fluid inclusions in South Indian granulites: evidence for entrapment during charnockite formation. Contributions to Mineralogy and Petrology 108, 318–330.

Schmidt-Mumm, A., Oberthür, T., Vetter, U., Blenkinsop, T.G., 1997. High CO_2 content of fluid inclusions in gold mineralisations in the Ashanti Belt, Ghana: a new category of ore forming fluids? Mineralium Deposita 32, 107–118.

Schwartz, M.O., Oberthür, T., Amanor, J., Gyapong, W.A., 1992. Fluid inclusion re-equililibration and P–T–X constraints on fluid evolution in the Ashanti gold deposit, Ghana. European Journal of Mineralogy 4, 1017–1033.

Seward, T.M., 1991. The geochemistry of gold. In: Foster, R.P. (Ed.), Gold Metallogeny and Exploration. Blackie & Son, Glasgow, pp. 37–62.

Shepherd, T.J., Rankin, A.H., Alderton, D.H., 1985. A practical guide for fluid inclusion studies. Blackie & Son, Glasgow. 239 pp.

Tassinari, C.C.G., Macambira, M.J.B., 1999. Geochronological provinces of the Amazonian Craton. Episodes 22, 174–182.

Touret, J.L.R., 1994. Fluid inclusions in sedimentary and diagenetic environments. In: De Vivo, B., Frezzotti, M.L. (Eds.), Fluid Inclusions in Minerals: Methods and Applications. Virginia Technical University, Blacksburg, pp. 251–269.

Vasquez, M.L., Lafon, J.M. 2001. Magmatismo tipo A de 1,75 Ga na porção oriental do Escudo das Guianas — Estados do Amapá e Pará, Brasil. In: Simpósio de Geologia da Amazônia, 7, Belém, Abstract volume CD-ROM.

Vityk, M.O., Bodnar, R.J., 1998. Statistical microthermometry of synthetic fluid inclusions in quartz during decompression reequilibration. Contributions to Mineralogy and Petrology 132, 149–162.

Walther, J.V., Orville, P.M., 1983. The extraction-quench technique for determination of the thermodynamic properties of solute complexes: application to quartz solubility in fluid mixtures. American Mineralogist 68, 731–741.

Watson, E.B., Brenan, J.M., 1987. Fluids in the lithosphere. 1. Experimentally determined wetting characteristics of CO2–H2O fluids and their implications for fluid transport, host-rock physical properties and fluid inclusion formation. Earth and Planetary Science Letters 85, 497–515.

Wilkinson, J.J., 2001. Fluid inclusions in hydrothermal ore deposits. Lithos 55, 229-172.

Wille, S.E., Klemd, R., 2004. Fluid inclusion studies of the Abawo gold prospect, near the Ashanti Belt, Ghana. Mineralim Deposita 39, 31–45.

Wilmart, E., Clocchiatti, R., Duchesne, J.C., Touret, J.L.R., 1991. Fluid inclusions in charnockites from the Bjerkreim–Sokndal massif (Rogaland, southwestern Norway): fluid origin and in situ evolution. Contributions to Mineralogy and Petrology 108, 453–462.

Xavier, R.P., Foster, R.P., 1999. Fluid evolution and chemical controls in the Fazenda Maria Preta (FMP) gold deposit, Rio Itapecuru Greenstone Belt, Bahia, Brazil. Chemical Geology 154, 133–154.

Xu, G., Pollard, P.J., 1999. Origin of CO_2-rich fluid inclusions in synorogenic veins from the Eastern Mount Isa Fold Belt, NW Queensland, and their implications for mineralization. Mineralium Deposita 34, 395–404.